

Two-color quark matter: $U(1)_A$ restoration, superfluidity, and quarkyonic phase

Tomáš Brauner^{*,1,†} Kenji Fukushima,² and Yoshimasa Hidaka³

¹*Institut für Theoretische Physik, Goethe-Universität,
Max-von-Laue-Straße 1, D-60438 Frankfurt am Main, Germany*

²*Yukawa Institute for Theoretical Physics, Kyoto University, Kyoto 606-8502, Japan*

³*Department of Physics, Kyoto University, Kyoto 606-8502, Japan*

We discuss the phase structure of quantum chromodynamics (QCD) with two colors and two flavors of light quarks. This is motivated by the increasing interest in the QCD phase diagram as follows: (1) The QCD critical point search has been under intensive dispute and its location and existence suffer from uncertainty of effective $U(1)_A$ symmetry restoration. (2) A new phase called quarkyonic matter is drawing theoretical and experimental attention but it is not clear whether it can coexist with diquark condensation. We point out that two-color QCD is nontrivial enough to contain essential ingredients for (1) and (2) both, and most importantly, is a system without the sign problem in numerical simulations on the lattice. We adopt the two-flavor Nambu–Jona-Lasinio model extended with the two-color Polyakov loop and make quantitative predictions which can be tested by lattice simulations.

PACS numbers: 11.10.Wx, 11.30.Rd, 12.38.Aw

Keywords: Quantum Chromodynamics, Effective Model, Chiral Symmetry, Color Deconfinement, Superfluidity, Finite Temperature, Finite Density

I. INTRODUCTION

Understanding the phase structure of quantum chromodynamics (QCD) is one of the key issues in current high-energy physics. Thorough phenomenological knowledge of properties of the hadron spectrum as well as nuclear matter is now being complemented by increasingly precise first-principle numerical studies of QCD at nonzero temperature. However, the application of lattice techniques to matter at high baryon chemical potential μ_B remains a major challenge due to the infamous sign problem [1]. The difficulties encountered in simulations of QCD triggered interest in similar theories which are free of the sign problem. These include simulations at imaginary chemical potential [2–13], QCD at nonzero isospin density [14–16], a QCD-like theory with adjoint quarks [17–20], and two-color QCD [21–33]. The latter, two-color QCD, will be the subject of the present article.

Two-color QCD differs in several aspects from the world we live in. The most notable difference perhaps is that the colorless baryons are formed from two quarks, and hence are bosons. Dense matter is then not realized as an interacting Fermi sea of nucleons, but rather as a Bose gas of diquarks which undergoes Bose–Einstein condensation (BEC) at sufficiently low temperature. Therefore the ground state of cold and dense two-color quark matter forms a superfluid [34]. Another noteworthy feature of two-color QCD, stemming from the fact that the $SU(2)$ gauge group has only pseudo-real representations, is the Pauli–Gürsey symmetry [35] connecting

quarks with antiquarks. As a consequence, the spectrum of Nambu–Goldstone (NG) bosons of the spontaneously broken chiral symmetry contains diquark states in addition to the pseudoscalar mesons. The presence of light particles carrying baryon number (i.e. baryonic pions) is quite peculiar to two-color QCD (and QCD with adjoint quarks) and crucial for understanding the phase structure at $T \neq 0$ and $\mu_B \neq 0$ by means of the chiral Lagrangian approach [17, 18, 36–38]. The model-independent chiral Lagrangian arguments have been complemented by investigations in various models such as the linear sigma model [39, 40], the random matrix theory [41–43], the strong-coupling expansion [28, 44–47]. The Nambu–Jona-Lasinio (NJL) model was first applied to two-color QCD in Ref. [48].

In fact there has been a tight communication between a number of effective model studies and the Monte-Carlo simulations on the lattice. Recent progress in this direction led to first attempts to probe BEC of diquarks and the region of moderate baryon density [29, 32]. Thus, based on the knowledge achieved in these preceding papers, the present paper aims to make a proposal to use the two-color QCD model as a controllable test setting to clarify the following controversial issues on the real-QCD phase diagram.

— In-medium $U(1)_A$ Symmetry Restoration —

The QCD Lagrangian has global $U(1)_A$ symmetry at the classical level. The quantum anomaly, however, leads to a nonconserving contribution to the axial current, which breaks $U(1)_A$ symmetry explicitly. From the point of view of quantum field theory the anomaly comes from highly ultraviolet modes, and thus, the anomaly should be insensitive to any infrared scales such as T , μ_B , and the quark mass m_0 . In this sense the $U(1)_A$ anomaly is never restored at any T nor μ_B . In the effective model description the $U(1)_A$ anomaly manifests itself in the form

^{*}On leave from Department of Theoretical Physics, Nuclear Physics Institute ASCR, CZ-25068 Řež, Czech Republic

[†]Electronic address: brauner@ujf.cas.cz

of a $U(1)_A$ -breaking interaction which is microscopically induced by instantons [49]. Because instantons are suppressed at high T or μ_B [50, 51], the $U(1)_A$ -breaking interaction is anticipated to weaken in a medium, leading to “effective restoration” of the $U(1)_A$ symmetry [52–56]. In fact, a quantitative estimate of the reduction of the $U(1)_A$ effect is crucial for locating the QCD critical point in the $\mu_B - T$ phase diagram [57–59]. The numerical study by the lattice Monte-Carlo simulation is in principle possible in two-color QCD. The clear signal for $U(1)_A$ restoration is degeneracy in the spectra of mesons connected by a $U(1)_A$ rotation [53]. That is, in the two-flavor case, the $U(1)_A$ partners are

$$\begin{cases} \text{Scalar-isoscalar } (\sigma) \text{ meson,} \\ \text{Pseudoscalar-isoscalar } (\eta_0) \text{ meson,} \\ \text{Scalar-isovector } (\vec{a}_0) \text{ meson,} \\ \text{Pseudoscalar-isovector } (\vec{\pi}) \text{ meson.} \end{cases}$$

The masses of these multiplets become degenerate when the chiral symmetry is also restored.

Since the σ meson involves the so-called disconnected diagrams, the lattice simulation is too noisy to see the degeneracy with η_0 (flavor-singlet η) which is also in a noisy channel. It is, however, feasible to check the degeneracy between \vec{a}_0 and $\vec{\pi}$ in the finite- T and finite- μ_B lattice simulation of two-color QCD. In this paper we will give a quantitative guide from an effective model study.

— Superfluidity and Quarkyonic Matter —

A new state of matter at high density has been recognized and it is now referred to as *quarkyonic matter* [60, 61]. Because the definition of quarkyonic matter is clear only in the large N_c limit, in which color non-singlet interactions are subleading, there seem to be some confusing arguments like that quarkyonic matter overwhelms color superconductivity. This is not quite true especially when N_c is finite. Intuitively, quarkyonic matter is characterized by the properties that the thermodynamic quantities (pressure, baryon density, etc.) should be almost saturated by the degenerated Fermi liquid of quarks and the collective excitations on top of the Fermi surface should be colorless (i.e. color confined). This is actually one of the known properties fulfilled by a certain color-superconducting phase, that is, the color-flavor locked (CFL) phase [62–65]. To form a colorless object in the CFL phase, however, we need to treat a meson composed of four quarks, which is technically complicated. Instead of real QCD, here, we shall make use of the two-color system; this exhibits superfluidity at high density which is reminiscent of color superconductivity in QCD, and besides, we need not treat four quarks, since diquarks (that is, baryons in the two-color world) can make a color singlet. We will demonstrate that the realization of quarkyonic matter is not so exclusive to disfavor superfluidity and diquark condensation. The goal of our discussions in this part is to make convincing the phase diagram as drawn in Fig. 1.

Let us now specify the model that we will use. Physics

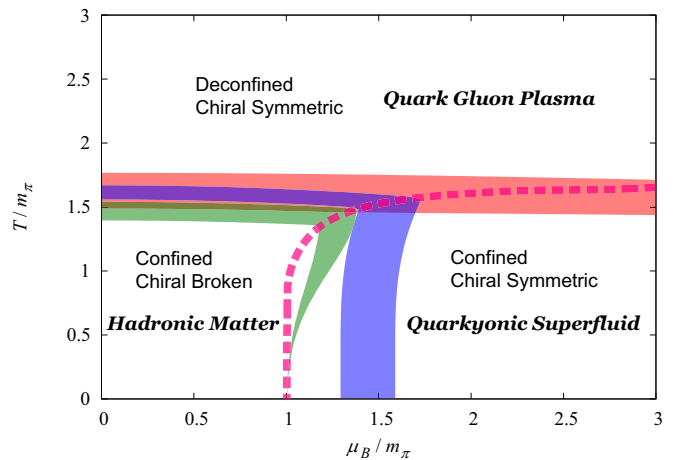


FIG. 1: Phase diagram of two-color QCD with two light quark flavors. The red and blue bands represent the regions in which the Polyakov loop and the normalized chiral condensate, respectively, take a value ranging from 0.4 to 0.6. The red dashed line extending from the bottom to the right shows the onset of diquark condensation. The green band surrounding the left-bottom corner indicates the region where n_B normalized by the “Stefan-Boltzmann” (see Sec. III B for detailed explanations) value ranges from 0.4 to 0.6.

of Cooper pairing of quarks (dense fermionic matter in general) is well described by NJL-type effective models. However, the NJL-type models suffer from a serious drawback: the lack of confinement, which may bring about artificial model predictions. In order to capture the essential features of confinement physics and yet maintain the technical simplicity of the NJL model, it was augmented with the Polyakov loop, equipped with a phenomenological potential designed to reproduce selected lattice data at finite T and zero μ_B [58, 66–72]. (See also, Ref. [73] for example, for a related approach of the Polyakov loop extended quark-meson model.) This extended model is now called the PNJL model. In spite of its simplicity, the PNJL model has shown remarkable agreement with thermodynamic quantities measured in the lattice QCD simulations. So far, among available finite- T and finite- μ_B model options at least, the PNJL model is one of the best tools to unveil the QCD phase structure. In this paper, in a sense, we *downgrade* the PNJL model into the two-color setting, hoping that our model predictions would guide the future two-color simulations.

Figure 1 is actually the phase diagram of two-color two-flavor QCD predicted by means of the PNJL model. We note that the phase diagram is divided into three regimes: One at high T consists of deconfined and chiral symmetric particles, which is to be identified as a quark-gluon plasma. The other one at low T and low μ_B is of course the hadronic phase. The last one at low T and high μ_B is commonly referred to as a superfluid state. We will later discuss that this state can be regarded as quarkyonic matter – so to speak, quarkyonic superfluid

of two-color quark matter. Keeping in mind this phase structure, we will look at the pole and screening masses of mesons to extract the information on $U(1)_A$ symmetry. The meson spectrum in the PNJL model was first analyzed in Ref. [69]. Along the same line, we will perform the calculations and examine the dependence of meson spectrum on the $U(1)_A$ -breaking interaction strength.

The paper is organized as follows. In Sec. II we introduce the model Lagrangian and derive some basic analytic formulas. Before going into the numerical study, we describe in Sec. III A in detail the way we fix the parameters of our model. Most of the results have been obtained numerically and are presented in Sec. III. Finally, in Sec. IV we summarize and conclude.

II. MODEL SETUP

Two-color QCD with N_f massless quark flavors has a global $U(2N_f)$ flavor invariance at the classical level owing to the Pauli–Gürsey symmetry [35]. The axial anomaly explicitly breaks $U(2N_f)$ to $SU(2N_f)$. In the vacuum, the $SU(2N_f)$ symmetry is spontaneously broken by the standard chiral condensate down to its $Sp(2N_f)$ subgroup. In the $N_f = 2$ case, which is the subject of the present paper, the symmetry-breaking pattern can be equivalently cast as $SO(6) \rightarrow SO(5)$ [34, 35]. The spectrum of NG modes therefore consists of a single 5-plet, including three pions and two diquarks (a diquark and an antidiquark – a baryonic and an antibaryonic pion). Within the NJL model, this degeneracy is reflected by the equality of couplings in the meson and diquark channels [48].

Let us begin the NJL analysis with the $U(1)_A$ -invariant interaction Lagrangian,

$$\mathcal{L}_1 = (1-\alpha)G \left[(\bar{\psi}\psi)^2 + (\bar{\psi}i\gamma_5\vec{\tau}\psi)^2 + (\bar{\psi}i\gamma_5\psi)^2 + (\bar{\psi}\vec{\tau}\psi)^2 + |\bar{\psi}^c\gamma_5\sigma_2\tau_2\psi|^2 + |\bar{\psi}^c\sigma_2\tau_2\psi|^2 \right], \quad (1)$$

where $\vec{\sigma}$ and $\vec{\tau}$ denote Pauli matrices in color and flavor spaces, and ψ^c the charge conjugation of the Dirac spinor $\psi^c = C\bar{\psi}^T$ with $C = i\gamma^2\gamma^0$. The interaction \mathcal{L}_1 is minimal in the sense that it only involves the scalar and pseudoscalar channels with isospin zero and unity. While the above \mathcal{L}_1 is invariant under a $U(1)_A$ rotation, we further need an interaction which breaks the $U(1)_A$ symmetry. To that end we consider the analogous interaction as follows:

$$\mathcal{L}_2 = \alpha G \left[(\bar{\psi}\psi)^2 + (\bar{\psi}i\gamma_5\vec{\tau}\psi)^2 - (\bar{\psi}i\gamma_5\psi)^2 - (\bar{\psi}\vec{\tau}\psi)^2 + |\bar{\psi}^c\gamma_5\sigma_2\tau_2\psi|^2 - |\bar{\psi}^c\sigma_2\tau_2\psi|^2 \right]. \quad (2)$$

The general interaction Lagrangian is thus a sum of these two; $\mathcal{L}_{\text{int}} = \mathcal{L}_1 + \mathcal{L}_2$. At $\alpha = 0$ only \mathcal{L}_1 remains and the interaction preserves $U(1)_A$, whereas at $\alpha = 1$ the remaining piece \mathcal{L}_2 breaks $U(1)_A$ maximally, being equivalent to the two-flavor instanton-induced interaction [34].

Indeed α is a usually used $U(1)_A$ -violating parameter [74] but we will also use $\zeta \equiv 1 - 2\alpha$ for notation simplicity. In previous works, $\zeta = 0$ ($\alpha = 1/2$) was used to discuss the phase structure [48, 75].

Performing the Hubbard–Stratonovich transformation in all six channels, we arrive at the total Lagrangian as

$$\begin{aligned} \mathcal{L} = & \bar{\psi}(i\gamma^\mu D_\mu - m_0 + \gamma_0\mu - \sigma - i\gamma_5\vec{\tau}\cdot\vec{\pi} - i\zeta\gamma_5\eta - \zeta\vec{\tau}\cdot\vec{a})\psi \\ & + \frac{1}{2} \left(\Delta^* \bar{\psi}^c i\gamma_5 \sigma_2 \tau_2 \psi + \text{h.c.} \right) + \frac{\zeta}{2} \left(\Delta_5^* \bar{\psi}^c i\sigma_2 \tau_2 \psi + \text{h.c.} \right) \\ & - \frac{1}{4G} (\sigma^2 + \vec{\pi}^2 + \zeta\eta^2 + \zeta\vec{a}^2 + |\Delta|^2 + \zeta|\Delta_5|^2). \quad (3) \end{aligned}$$

The covariant derivative D_μ involves coupling of the quarks to the background gauge field A_4 which translates to the Polyakov loop in the end. In addition, we note that m_0 and μ denote the current quark mass and the quark chemical potential. Later we will introduce μ_B to denote the baryon chemical potential; $\mu_B = 2\mu$ where 2 comes from the number of colors. The collective fields $\sigma, \vec{\pi}, \eta, \vec{a}, \Delta, \Delta_5$ represent in order the mesons in the scalar-isoscalar, pseudoscalar-isovector, pseudoscalar-isoscalar, and scalar-isovector channels, and the scalar and pseudoscalar diquarks. (We hereafter omit the subscript “0” out of η_0 and \vec{a}_0 for simplicity.)

In the absence of isospin chemical potential the isovector modes do not develop a vacuum expectation value. Moreover, the Vafa–Witten theorem [76] guarantees that the chiral condensate in the vacuum has positive parity. In our model approach, this requires $\alpha \geq 0$, that is, $\zeta \leq 1$. (At the same time, $\zeta \geq 0$, i.e., $\alpha \leq 1/2$ is needed for our mean-field treatment using the Hubbard–Stratonovich transformation [77].) Consequently, with the exception of the $U(1)_A$ -conserving limit $\alpha = 0$, the scalar chiral and diquark condensates will always be preferred to the pseudoscalar ones. We will therefore take into account only the σ and Δ condensates. The mean-field thermodynamics of the system is then independent of the parameter α , which will only affect the propagation of collective modes, to be discussed in Sec. II B.

A. Thermodynamics

In the PNJL model, one introduces a constant temporal gauge field which couples to the quarks via the covariant derivative. In the Polyakov gauge this gauge field is diagonal in the color space, and for the color $SU(2)$ group it has a form, $A_4 = iA_0 = \sigma_3\theta$, where θ is a real “phase”. The order parameter for deconfinement is then the traced Polyakov loop given by

$$\Phi = \frac{1}{N_c} \text{Tr} e^{i\beta A_4} = \cos(\beta\theta), \quad (4)$$

where β is the inverse temperature. In the mean-field approximation, the thermodynamic potential is given by a sum of the gauge and quark parts,

$$\Omega = \Omega_{\text{gauge}} + \Omega_{\text{quark}}. \quad (5)$$

In the following, we will refer to the two quark colors for simplicity as the “red” and “green”. Combining the red quark and the green antiquark into the Nambu–Gor’kov spinor, $\Psi = (\psi_r, \tau_2 \psi_g^c)^T$, the background gauge field becomes proportional to the unit matrix in this doubled space and the quark thermodynamic potential can be expressed as

$$\Omega_{\text{quark}} = \frac{\sigma^2 + \Delta^2}{4G} - T \sum_n \int \frac{d^3 \mathbf{k}}{(2\pi)^3} \text{Tr} \log(i\omega_n - i\theta - \mathcal{H}_{\mathbf{k}}), \quad (6)$$

where the Nambu–Gor’kov Hamiltonian reads

$$\mathcal{H}_{\mathbf{k}} = \begin{pmatrix} \boldsymbol{\alpha} \cdot \mathbf{k} + \gamma_0 M - \mu & -\gamma_0 \gamma_5 \Delta \\ \gamma_0 \gamma_5 \Delta^* & \boldsymbol{\alpha} \cdot \mathbf{k} + \gamma_0 M + \mu \end{pmatrix}. \quad (7)$$

Here $M = m_0 + \sigma$ is the constituent quark mass and the σ and Δ now stand for the condensates. The four eigenvalues of the Hamiltonian are easily found as $+E_{\mathbf{k}}^{\pm}$ and $-E_{\mathbf{k}}^{\pm}$ corresponding to the gapped quasiparticle dispersion relations, where

$$E_{\mathbf{k}}^{\pm} = \sqrt{(\xi_{\mathbf{k}}^{\pm})^2 + \Delta^2}, \quad (8)$$

$$\xi_{\mathbf{k}}^{\pm} = \epsilon_{\mathbf{k}} \pm \mu, \quad \epsilon_{\mathbf{k}} = \sqrt{\mathbf{k}^2 + M^2}.$$

The total thermodynamic potential thus becomes

$$\Omega = -bT [24\Phi^2 e^{-\beta a} + \log(1 - \Phi^2)] + \frac{\sigma^2 + \Delta^2}{4G} - 4 \sum_{i=\pm} \int \frac{d^3 \mathbf{k}}{(2\pi)^3} \left[E_{\mathbf{k}}^i + T \log \left(1 + 2\Phi e^{-\beta E_{\mathbf{k}}^i} + e^{-2\beta E_{\mathbf{k}}^i} \right) \right]. \quad (9)$$

The first term is the gauge part Ω_{gauge} having two model parameters a and b . We assume the simple form motivated by lattice strong-coupling expansion [58]. It differs from the three-color expression by a simpler logarithmic term due to the SU(2) Haar measure, and by the rescaled prefactor of the exponential term, which is in general proportional to N_c^2 . Note that, as usual in the PNJL model literature, we simulate the effects of gauge dynamics by a constant background temporal gauge field. We then adopt a phenomenological ansatz for the gauge contribution to the mean-field thermodynamic potential, chosen to reproduce selected features of the pure gauge theory. Therefore, the parameters a, b only enter the thermodynamic potential (9) since there are no dynamical gauge degrees of freedom in our model Lagrangian (3).

It is interesting to recall that in the three-color case the thermodynamic potential in general cannot be written in terms of the Polyakov loop variable Φ (and the conjugate $\bar{\Phi}$) only, and one has to use two phases analogous to our θ to parameterize it. On the contrary, in the two-color PNJL model the thermodynamic potential depends just on Φ even in the presence of a diquark condensate.

This is because diquarks are colorless. This consideration simplifies the discussion and also avoids technical ambiguities stemming from generally complex effective actions involving the diquark condensate [68, 71, 72, 78]. The values of the condensates in thermodynamic equilibrium are determined by minimizing the thermodynamic potential with respect to the variables σ , Δ , and Φ .

In the quark sector, the effect of the Polyakov loop as compared to the simple NJL model is to make the replacement $E + 2T \log(1 + e^{-\beta E}) \rightarrow E + T \log(1 + 2\Phi e^{-\beta E} + e^{-2\beta E})$ in the quasiparticle contribution to the thermodynamic potential. Similarly, in the gap equations as well as collective mode propagators, one generalizes $1 - 2f(E) = \tanh(\beta E/2)$, where $f(E) = 1/(e^{\beta E} + 1)$ is the Fermi–Dirac distribution, to

$$\varphi(E) \equiv \frac{\sinh(\beta E)}{\cosh(\beta E) + \Phi} = \left(1 + \frac{1 - \Phi}{\cosh(\beta E) + \Phi} \right) [1 - 2f(E)] \quad (10)$$

$$= \left(1 - \frac{\Phi}{\cosh(\beta E) + \Phi} \right) [1 - 2f(2E)]. \quad (11)$$

The latter two forms (10) and (11) of the function $\varphi(x)$ illustrate that for $\Phi \rightarrow 1$ thermal excitations are dominated by quark modes with baryon number 1/2 (i.e. deconfinement), while for $\Phi \rightarrow 0$ by baryon modes with baryon number 1 (i.e. confinement). With these replacements, one can readily generalize the results of the pure NJL model to the Polyakov loop-extended one, as observed in Ref. [69] for the three-color case.

At zero temperature the Polyakov loop expectation value is zero for all values of the chemical potential. This led to the suggestion that the PNJL model can naturally describe quarkyonic matter [60, 61] at high chemical potential, that is, a phase where chiral symmetry is restored but confinement persists [58, 73, 79]. A simple glance at Eq. (9) shows that when $\Phi = 0$, thermal excitations are indeed governed by the term $e^{-2\beta E_{\mathbf{k}}^e}$, i.e., they correspond to colorless baryons. Let us take a closer look at how $\Phi \simeq 0$ arises as $T \rightarrow 0$.

We consider the gap equation for Φ following from Eq. (9), that is,

$$b\Phi \left(\frac{1}{1 - \Phi^2} - 24e^{-\beta a} \right) = \sum_{i=\pm} \int \frac{d^3 \mathbf{k}}{(2\pi)^3} \frac{2}{\Phi + \cosh(\beta E_{\mathbf{k}}^i)}. \quad (12)$$

At high enough μ and low T the system is in the Bardeen–Cooper–Schrieffer (BCS) regime where Cooper pairing of quarks occurs close to the Fermi sea [75]. The right-hand side of this equation is then dominated by the particle ($i = -$) part. We can further simplify the calculation by using the high-density approximation, in which we expand the dispersion relation around the Fermi surface, $E^- = \sqrt{\xi^2 + \Delta^2} \approx \Delta + \xi^2/(2\Delta)$, and replace the measure $d^3 \mathbf{k}/(2\pi)^3$ by $\mathcal{N} d\xi$, where $\mathcal{N} = \mu k_F/(2\pi^2)$ is the density of states at the Fermi surface. The integral thus becomes

Gaussian near $T \simeq 0$ and we arrive at the asymptotic result as

$$\Phi_{\text{BCS}} \approx \frac{4\mathcal{N}}{b} e^{-\beta\Delta} \sqrt{2\pi\Delta T}. \quad (13)$$

The Polyakov loop itself is hence suppressed exponentially at low temperature.

B. Collective modes

The propagators of the collective modes are easily obtained by a second variation of the effective action that follows from Eq. (3) after integrating the quarks fields out. Denoting a set of collective fields symbolically as χ_i , the inverse propagator at imaginary (bosonic Matsubara) frequency $i\omega'_m$ is given by

$$D_{ij}^{-1}(i\omega'_m, \mathbf{p}) = C_i \delta_{ij} + T \sum_n \int \frac{d^3 \mathbf{k}}{(2\pi)^3} \times \text{Tr} \left[\frac{\partial \mathcal{H}}{\partial \chi_i} \frac{1}{i(\tilde{\omega}_n + \omega'_m) - \mathcal{H}_{\mathbf{k}+\frac{\mathbf{p}}{2}}} \frac{\partial \mathcal{H}}{\partial \chi_j} \frac{1}{i\tilde{\omega}_n - \mathcal{H}_{\mathbf{k}-\frac{\mathbf{p}}{2}}} \right], \quad (14)$$

where $\tilde{\omega}_n = \omega_n - \theta$ and ω_n stands for the fermionic Matsubara frequencies. The constant C_i is equal to $1/(2G)$ for $\sigma, \vec{\pi}$, to $1/(4G)$ for Δ, Δ^* , to $\zeta/(2G)$ for η, \vec{a} , and to $\zeta/(4G)$ for Δ_5, Δ_5^* . The trace is taken in Dirac, flavor, as well as Nambu–Gor’kov space. When calculating the partial derivatives of the Hamiltonian, that determine the Yukawa couplings of quarks to the bosonic modes, we demand that all fields have to be kept as in Eq. (3).

In the diquark condensation phase, the baryon number is spontaneously broken. As a result some of the modes mix and we have to find their dispersion relations by diagonalizing a matrix propagator. This applies to the scalar-isoscalar modes, σ, Δ, Δ^* , as well as pseudoscalar-isoscalar modes, $\eta, \Delta_5, \Delta_5^*$. The only modes that do not mix are $\vec{\pi}$ and \vec{a} thanks to conservation of isospin and parity. Their inverse propagators are trivial in isospin space, namely, $D_{ij}^{-1} = \delta_{ij} D_i^{-1}$. After analytic continuation to real frequencies they acquire the following forms:

$$\begin{aligned} D_{\pi}^{-1}(\omega, \mathbf{p}) &= \frac{1}{2G} - \sum_{i,j=\pm} \sum_{k,l=\pm} \int \frac{d^3 \mathbf{q}}{(2\pi)^3} \frac{1}{2E_{\mathbf{q}+\frac{\mathbf{p}}{2}}^i E_{\mathbf{q}-\frac{\mathbf{p}}{2}}^{-j}} \left(1 + ij \frac{\epsilon_{\mathbf{q}}^2 - \frac{\mathbf{p}^2}{4}}{\epsilon_{\mathbf{q}+\frac{\mathbf{p}}{2}} \epsilon_{\mathbf{q}-\frac{\mathbf{p}}{2}}} \right) \\ &\quad \times \frac{(E_{\mathbf{q}+\frac{\mathbf{p}}{2}}^i + ik \xi_{\mathbf{q}+\frac{\mathbf{p}}{2}}^i)(E_{\mathbf{q}-\frac{\mathbf{p}}{2}}^{-j} + jl \xi_{\mathbf{q}-\frac{\mathbf{p}}{2}}^{-j}) + kl \Delta^2}{\omega + kE_{\mathbf{q}+\frac{\mathbf{p}}{2}}^i + lE_{\mathbf{q}-\frac{\mathbf{p}}{2}}^{-j}} \left[\varphi(kE_{\mathbf{q}+\frac{\mathbf{p}}{2}}^i) + \varphi(lE_{\mathbf{q}-\frac{\mathbf{p}}{2}}^{-j}) \right], \\ D_a^{-1}(\omega, \mathbf{p}) &= \frac{\zeta}{2G} - \zeta^2 \sum_{i,j=\pm} \sum_{k,l=\pm} \int \frac{d^3 \mathbf{q}}{(2\pi)^3} \frac{1}{2E_{\mathbf{q}+\frac{\mathbf{p}}{2}}^i E_{\mathbf{q}-\frac{\mathbf{p}}{2}}^{-j}} \left(1 - ij \frac{M^2 - \mathbf{q}^2 + \frac{\mathbf{p}^2}{4}}{\epsilon_{\mathbf{q}+\frac{\mathbf{p}}{2}} \epsilon_{\mathbf{q}-\frac{\mathbf{p}}{2}}} \right) \\ &\quad \times \frac{(E_{\mathbf{q}+\frac{\mathbf{p}}{2}}^i + ik \xi_{\mathbf{q}+\frac{\mathbf{p}}{2}}^i)(E_{\mathbf{q}-\frac{\mathbf{p}}{2}}^{-j} + jl \xi_{\mathbf{q}-\frac{\mathbf{p}}{2}}^{-j}) - kl \Delta^2}{\omega + kE_{\mathbf{q}+\frac{\mathbf{p}}{2}}^i + lE_{\mathbf{q}-\frac{\mathbf{p}}{2}}^{-j}} \left[\varphi(kE_{\mathbf{q}+\frac{\mathbf{p}}{2}}^i) + \varphi(lE_{\mathbf{q}-\frac{\mathbf{p}}{2}}^{-j}) \right]. \end{aligned} \quad (15)$$

Here, we have changed the momentum notation from \mathbf{k} to \mathbf{q} to reserve k to take a summation over \pm . It should be noted that in the limit $|\mathbf{p}| \rightarrow 0$, only the $i = j$ terms survive and the expressions somewhat simplify. The first of the formulas can be used together with the gap equation for Δ to show that in the diquark condensation phase the pion (pole) mass is exactly equal to $2\mu = \mu_B$ at zero temperature. The proof is straightforward, hence we omit the details.

In the normal phase (where $\Delta = 0$) all propagators can be evaluated easily. We provide here the list of expressions that we later in Sec. III C use to calculate the masses numerically. To recall that these are the propagators in normal

matter, let us write a superscript (n):

$$\begin{aligned}
D_\sigma^{(n)-1}(\omega, \mathbf{p}) &= \frac{1}{2G} - 2 \sum_{i,j=\pm} \int \frac{d^3 \mathbf{k}}{(2\pi)^3} \left(1 - ij \frac{M^2 - \mathbf{k}^2 + \frac{\mathbf{p}^2}{4}}{\epsilon_{\mathbf{k}+\frac{\mathbf{p}}{2}} \epsilon_{\mathbf{k}-\frac{\mathbf{p}}{2}}} \right) \frac{\varphi(i \xi_{\mathbf{k}+\frac{\mathbf{p}}{2}}^i) + \varphi(j \xi_{\mathbf{k}-\frac{\mathbf{p}}{2}}^{-j})}{\omega + i \epsilon_{\mathbf{k}+\frac{\mathbf{p}}{2}} + j \epsilon_{\mathbf{k}-\frac{\mathbf{p}}{2}}}, \\
D_\pi^{(n)-1}(\omega, \mathbf{p}) &= \frac{1}{2G} - 2 \sum_{i,j=\pm} \int \frac{d^3 \mathbf{k}}{(2\pi)^3} \left(1 + ij \frac{\epsilon_{\mathbf{k}}^2 - \frac{\mathbf{p}^2}{4}}{\epsilon_{\mathbf{k}+\frac{\mathbf{p}}{2}} \epsilon_{\mathbf{k}-\frac{\mathbf{p}}{2}}} \right) \frac{\varphi(i \xi_{\mathbf{k}+\frac{\mathbf{p}}{2}}^i) + \varphi(j \xi_{\mathbf{k}-\frac{\mathbf{p}}{2}}^{-j})}{\omega + i \epsilon_{\mathbf{k}+\frac{\mathbf{p}}{2}} + j \epsilon_{\mathbf{k}-\frac{\mathbf{p}}{2}}}, \\
D_\eta^{(n)-1}(\omega, \mathbf{p}) &= \frac{\zeta}{2G} - 2\zeta^2 \sum_{i,j=\pm} \int \frac{d^3 \mathbf{k}}{(2\pi)^3} \left(1 + ij \frac{\epsilon_{\mathbf{k}}^2 - \frac{\mathbf{p}^2}{4}}{\epsilon_{\mathbf{k}+\frac{\mathbf{p}}{2}} \epsilon_{\mathbf{k}-\frac{\mathbf{p}}{2}}} \right) \frac{\varphi(i \xi_{\mathbf{k}+\frac{\mathbf{p}}{2}}^i) + \varphi(j \xi_{\mathbf{k}-\frac{\mathbf{p}}{2}}^{-j})}{\omega + i \epsilon_{\mathbf{k}+\frac{\mathbf{p}}{2}} + j \epsilon_{\mathbf{k}-\frac{\mathbf{p}}{2}}}, \\
D_a^{(n)-1}(\omega, \mathbf{p}) &= \frac{\zeta}{2G} - 2\zeta^2 \sum_{i,j=\pm} \int \frac{d^3 \mathbf{k}}{(2\pi)^3} \left(1 - ij \frac{M^2 - \mathbf{k}^2 + \frac{\mathbf{p}^2}{4}}{\epsilon_{\mathbf{k}+\frac{\mathbf{p}}{2}} \epsilon_{\mathbf{k}-\frac{\mathbf{p}}{2}}} \right) \frac{\varphi(i \xi_{\mathbf{k}+\frac{\mathbf{p}}{2}}^i) + \varphi(j \xi_{\mathbf{k}-\frac{\mathbf{p}}{2}}^{-j})}{\omega + i \epsilon_{\mathbf{k}+\frac{\mathbf{p}}{2}} + j \epsilon_{\mathbf{k}-\frac{\mathbf{p}}{2}}}, \\
D_\Delta^{(n)-1}(\omega, \mathbf{p}) &= \frac{1}{4G} - \sum_{i,j=\pm} \int \frac{d^3 \mathbf{k}}{(2\pi)^3} \left(1 + ij \frac{\epsilon_{\mathbf{k}}^2 - \frac{\mathbf{p}^2}{4}}{\epsilon_{\mathbf{k}+\frac{\mathbf{p}}{2}} \epsilon_{\mathbf{k}-\frac{\mathbf{p}}{2}}} \right) \frac{\varphi(i \xi_{\mathbf{k}+\frac{\mathbf{p}}{2}}^i) + \varphi(j \xi_{\mathbf{k}-\frac{\mathbf{p}}{2}}^j)}{\omega + 2\mu + i \epsilon_{\mathbf{k}+\frac{\mathbf{p}}{2}} + j \epsilon_{\mathbf{k}-\frac{\mathbf{p}}{2}}}, \\
D_{\Delta_5}^{(n)-1}(\omega, \mathbf{p}) &= \frac{\zeta}{4G} - \zeta^2 \sum_{i,j=\pm} \int \frac{d^3 \mathbf{k}}{(2\pi)^3} \left(1 - ij \frac{M^2 - \mathbf{k}^2 + \frac{\mathbf{p}^2}{4}}{\epsilon_{\mathbf{k}+\frac{\mathbf{p}}{2}} \epsilon_{\mathbf{k}-\frac{\mathbf{p}}{2}}} \right) \frac{\varphi(i \xi_{\mathbf{k}+\frac{\mathbf{p}}{2}}^i) + \varphi(j \xi_{\mathbf{k}-\frac{\mathbf{p}}{2}}^j)}{\omega + 2\mu + i \epsilon_{\mathbf{k}+\frac{\mathbf{p}}{2}} + j \epsilon_{\mathbf{k}-\frac{\mathbf{p}}{2}}}.
\end{aligned} \tag{16}$$

Propagators of the antiquarks, Δ^* and Δ_5^* , are obtained from the diquark ones by charge conjugation, i.e. changing the sign of the chemical potential.

III. NUMERICAL RESULTS

Armed with these analytic expressions we are now ready to proceed in the numerical calculations. First we will explain our choice of the model parameters. Next we will investigate the phase diagram, in which we particularly look into the nature of the superfluid phase. Finally we will come to the discussion of the meson spectrum dependence on the $U(1)_A$ -breaking parameter α .

A. Parameter fixing

Our model has five parameters whose values have to be chosen appropriately: a and b in the Polyakov loop sector, and G , m_0 , and the sharp three-momentum cutoff Λ in the NJL sector. (The parameter α or ζ will be treated as an undetermined free parameter.)

Let us first concentrate on the latter. In the three-color NJL model one normally fixes the values of G , m_0 , and Λ from the physical pion mass m_π , decay constant f_π , which are both measured experimentally, and the chiral condensate, which is calculated on the lattice or estimated from the QCD sum rules [74]. The authors of Ref. [48] chose to set up the two-color NJL model using roughly the same input values, while in Ref. [75] the pion mass, decay constant and the (three-color) constituent quark mass were used, resulting in a rather different parameter set. We shall argue here that both these fits may

be actually overdetermined and one should be very careful especially when comparing the model outputs with lattice data.

The chiral limit QCD, as a Yang–Mills theory coupled to massless quarks in the color fundamental representation, has a single mass scale, namely Λ_{QCD} . All physical quantities should be expressed as an appropriate power of Λ_{QCD} times a dimensionless number. In the NJL model one can therefore choose freely a single input quantity, basically just to set the energy unit. Dimensionless combinations of observables are a pure prediction of QCD, and shall thus not be tuned to arbitrary values. In particular, either the pion decay constant, the chiral condensate, or the constituent quark mass may serve for this purpose, but not two of them independently. With the fact in mind that the current quark mass is a free parameter in the lattice simulation, we note that the pion mass can in principle acquire any value and represents a new physical scale in addition to Λ_{QCD} .

Unfortunately, we are not aware of any lattice data which would provide us with the input needed to fix the NJL model parameters unambiguously. In order to make at least an educated guess, we use an argument based on the N_c scaling of physical quantities. Using the fact that f_π is proportional to $\sqrt{N_c}$ and the chiral condensate to N_c , we rescale the three-color values by factors $\sqrt{2/3}$ and $2/3$, respectively. Regarding the Polyakov loop sector parameters, the constant a is related to the critical temperature T_c for deconfinement in the pure gauge theory by $a = T_c \log 24$. Since T_c in the first approximation does not depend on N_c [60], we use the value $T_c = 270$ MeV. The parameter b can in principle be adjusted in order to make the chiral and deconfinement crossovers happen at about the same temperature [58].

TABLE I: First two lines: physical quantities used as an input. Last two lines: fitted parameters of the model.

T_c [MeV]	$\sigma_s^{1/2}$ [MeV]	$-\langle\bar{\psi}_u\psi_u\rangle^{1/3}$ [MeV]	f_π [MeV]	m_π [MeV]
270	425	218	75.4	140
a [MeV]	$b^{1/3}$ [MeV]	Λ [MeV]	G [GeV $^{-2}$]	m_0 [MeV]
858.1	210.5	657	7.23	5.4

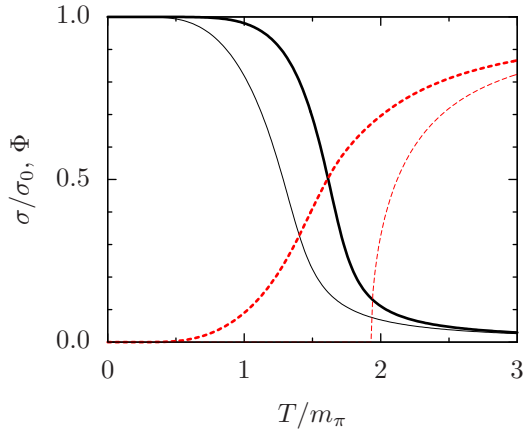


FIG. 2: Chiral and deconfinement crossovers at $\mu_B = 0$. The thick lines show the PNJL result (black solid: chiral condensate in units of the vacuum value σ_0 ; red dashed: Polyakov loop Φ), while the thin lines indicate the pure chiral (NJL) and pure gauge transitions. As expected, the deconfinement transition in the absence of quarks is of second order.

Here we use the estimate based on lattice strong-coupling expansion, $b = (\sigma_s/a)^3$, where $\sigma_s = (425 \text{ MeV})^2$ is the physical string tension. The input values as well as the fitted parameter set are summarized in Table I.

In order to check that our parameter set is reasonable, we plot in Fig. 2 the expectation values of σ and Φ as a function of T at $\mu_B = 0$. The positions of the two crossovers move very close to each other when the coupling between the quark and Polyakov loop sectors is switched on. We note that this observation of simultaneous crossovers is less clear if we use the unrescaled input parameters.

B. Phase diagram and diquark condensation

In the vacuum the diquark is degenerate with the pions and its mass is therefore m_π . Thus, when $\mu_B (= 2\mu)$ exceeds m_π , the diquark condenses and one enters the BEC phase which forms a superfluid component. At this moment the constituent quark mass M is still rather large. However, as μ_B further increases, M drops. Once $\mu > M$, a Fermi sea of quarks appears. Here we note that the baryon number density, n_B , acquires a contribution from the diquark condensate and becomes nonzero as soon as $\mu_B = m_\pi$ or $\mu = m_\pi/2$. Because of the binding energy,

naturally, $m_\pi/2$ is smaller than M , and thus the onset of $n_B \neq 0$ emerges first and then a quark Fermi sea shows up with increasing μ . In the presence of the Fermi sea the diquark condensation is closer to the BCS pairing of quarks sitting near the Fermi surface rather than to BEC of bound bosonic molecules. There is no phase transition associated with this qualitative change of behavior, so one speaks of a BCS–BEC crossover. Even though it is not particularly sharp, it can be conveniently defined by the condition $\mu = M$ [75].

We will draw the phase diagram of our model in a “conventional” way. In the phase diagram the deconfinement crossover is conveniently defined by the condition $\Phi = 0.5$. The deconfinement temperature is then almost independent of the chemical potential. In fact, the value of the Polyakov loop at all temperatures depends on μ_B very weakly, as can be seen from Fig. 3, where all condensates are plotted as a function of T/m_π and μ_B/m_π where m_π is fixed to be 140 MeV. This behavior of the Polyakov loop can be traced back to the fact that the two-color diquark is a color singlet, and therefore does not break center symmetry to induce nonzero Polyakov loop directly.

Even at nonzero quark mass the diquark condensate exhibits a clear second-order phase transition as shown in the plot for Δ/σ_0 (where σ_0 is the vacuum value of the chiral condensate) in Fig. 3. Unlike the deconfinement crossover, we can draw a well-defined phase boundary in the phase diagram separating the normal and superfluid phases. As we have already mentioned above, we can confirm that nonzero Δ certainly appears at $\mu_B = m_\pi$ at $T = 0$.

A compilation of these data leads to the phase diagram we present in Fig. 4. The solid line represents a second-order phase transition between the normal and superfluid phases. In the superfluid region we have added a dash-dotted line which indicates $\mu = M$ and can be interpreted as a BCS–BEC-type crossover. The dashed line is the deconfinement crossover defined by $\Phi = 0.5$. Figure 4 is a basis to understand a more “advocative” way of presenting the phase diagram as shown in Fig. 1.

Now we are well prepared to discuss the physical meaning of each phase labeled in Fig. 1. The red band which spreads almost straight along the horizontal axis represents the deconfinement crossover. Because a crossover has a width and does not have a unique definition, it should be much more reasonable to express the transition region not by a line but a band. The band width

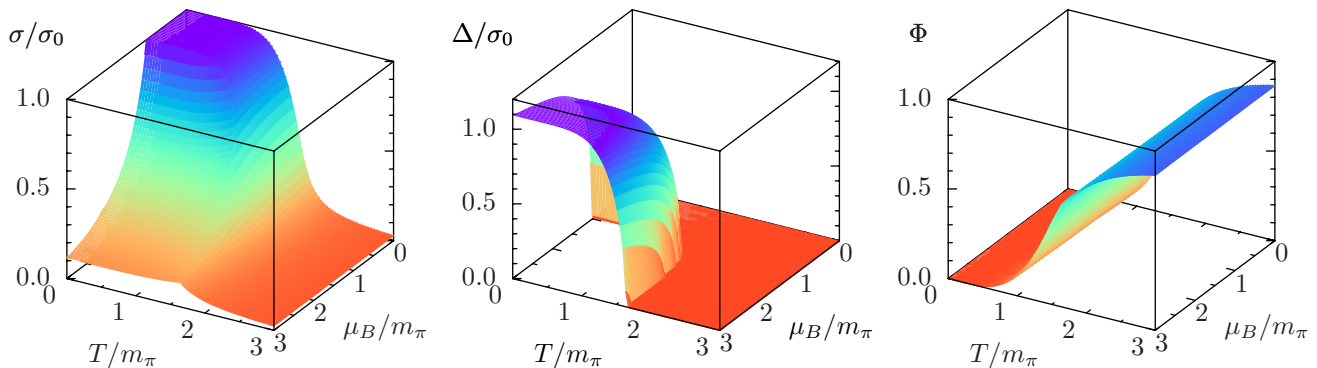


FIG. 3: Chiral condensate σ , diquark condensate Δ , which are given as divided by the chiral condensate in the vacuum σ_0 , and the Polyakov loop Φ as a function of μ_B and T in units of the pion mass $m_\pi = 140$ MeV. Note the orientation of the axes, chosen to obtain a better view of the surfaces!

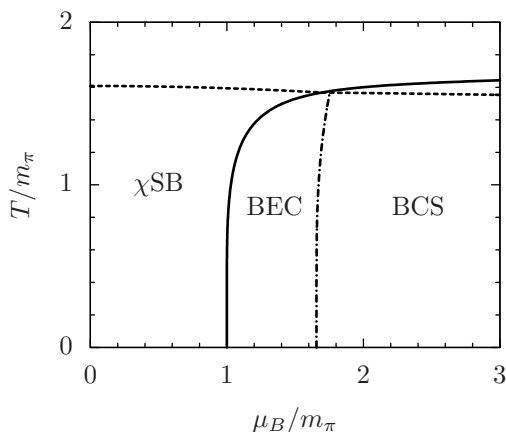


FIG. 4: Conventional presentation of the phase diagram of two-color QCD from the PNJL model in the $\mu_B - T$ plane. We indicate the chiral-symmetry breaking (χ SB), BEC, and BCS phases. Solid line: critical onset of diquark condensation where Δ starts to be nonzero. Dashed line: deconfinement crossover (defined by $\Phi = 0.5$). Dash-dotted line: BCS-BEC crossover (defined by $\mu = M$).

in fact tells us how rapid or slow the crossover is. We drew the deconfinement band by the condition that Φ ranges from 0.4 to 0.6. The blue band showing a sudden decrease around $\mu_B/m_\pi \simeq 1.5$ is the chiral crossover defined similarly by the condition that σ/σ_0 ranges from 0.4 to 0.6. We see that the two crossovers of deconfinement and chiral restoration take place simultaneously at zero density, and this coincidence persists until around $\mu_B/m_\pi \simeq 1.5$. The pink dotted line represents the superfluid onset, which is a well-defined phase transition. Finally the green band which shows behavior similar to the chiral crossover is drawn by the baryon number density n_B . We can compute n_B in the PNJL model and normalize it by the “Stefan-Boltzmann” value. Since the PNJL model is a cutoff theory, even the free (non-interacting) limit suffers from the cutoff artifact and deviates from the standard formula, which is also the case in the lattice simulation [80]. Therefore we evaluate the baryon

number density in the Stefan-Boltzmann limit $(n_B)_{\text{SB}}$ using the PNJL model with $M = 0$ and $\Phi = 1$ imposed by hand. In this way, we indicate by the green band in Fig. 1 the region in which $n_B/(n_B)_{\text{SB}}$ ranges from 0.4 to 0.6.

Because the chiral phase transition controls the dynamical quark mass, it is conceivable that the BCS-BEC crossover in Fig. 4 is associated with the chiral crossover. This is indeed the case; the dash-dotted line in Fig. 4 is covered by the chiral crossover band in Fig. 1. Hence, as labeled in Fig. 1, the right-bottom region is characterized by small Φ (confinement) and small σ/σ_0 (chiral symmetric). This is in fact in accord with the identification of quarkyonic matter in Refs. [58, 79]. In this case the blue band is interpreted as the quarkyonic transition. If we use $n_B/(n_B)_{\text{SB}}$ to define the quarkyonic transition according to Refs. [60, 81], the green band, instead of the blue band, plays the role of the quarkyonic boundary.

We would emphasize here that the former criterion makes more physical sense at least in the present case of $N_c = 2$. Actually, our consideration of the BCS-BEC crossover provides us with a clear view point on this issue. As we have already discussed, in the chemical potential window $1 \lesssim \mu_B/m_\pi \lesssim 1.5$, finite baryon number density grows. The carriers of the baryon number are, however, not quarks but baryons (baryonic pions). This is so because $m_\pi < \mu_B < 2M$ in this region. Therefore, in the phase region we called BEC in Fig. 4, the more appropriate physical interpretation should be “superfluid nuclear matter” rather than a quarkyonic state in which the pressure is mostly given by Fermi-degenerated quarks. This difference in the interpretation makes a contrast to the large- N_c arguments [60, 81], and it still remains a question to which the real world with $N_c = 3$ is closer, infinite N_c or $N_c = 2$? Answering this question goes beyond our current scope. If the quark-hadron continuity scenario driven by the CFL state is realistic, we can say that the situation at $N_c = 2$ is more relevant.

Before closing this section we mention the previous studies. In preceding works there was some controversy regarding the order of the phase transition from the di-

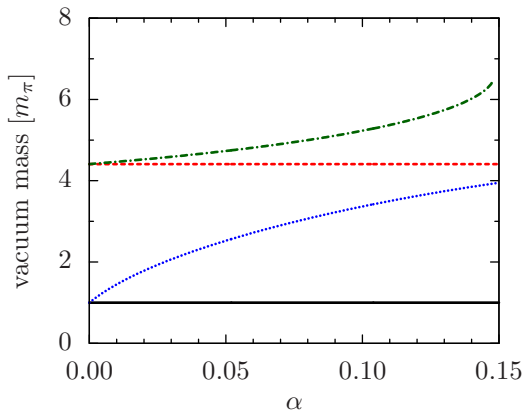


FIG. 5: Dependence of the vacuum meson masses on the $U(1)_A$ -breaking parameter α . The black solid is m_π , the red dashed m_σ , the blue dotted m_η , and the green dash-dotted m_a . We see that $m_\pi = m_\eta$ and $m_\sigma = m_a$ in the $U(1)_A$ symmetric ($\alpha = 0$) case.

quark condensation phase to the normal phase. In [48] it was concluded that there is a tricritical point at μ_B/m_π somewhere in the range 2.2 – 2.4, and for higher μ_B the transition becomes first order. On the other hand, the authors of [75] used the Thouless criterion to calculate the critical temperature, which *assumes* that the transition is second order. Our numerical results for the diquark condensate as a function of T/m_π and μ_B/m_π (see Fig. 3) suggest that the transition is second order everywhere. We have further confirmed the statement that there is no first-order phase transition by looking at the quartic Ginzburg–Landau coefficient in our numerical calculation. Detailed computations and arguments are given in the Appendix.

C. Collective mode spectrum

We are going to investigate the mass spectrum of collective modes as a function of T and μ_B for different values of the $U(1)_A$ -breaking parameter α . A useful starting point therefore is the α -dependence of the masses in the vacuum. This is shown in Fig. 5. It is worth noting that we only display the meson spectrum; thanks to the unbroken $SO(5)$ symmetry at $\mu_B = 0$, the scalar diquark Δ is degenerate with π mesons and the pseudoscalar diquark Δ_5 is degenerate with the a_0 mesons. We should perhaps emphasize that whenever we speak of a (pole) mass, we have in mind the zero of the real part of the inverse propagator [82]. We will therefore sometimes refer to it as the real-part mass. This coincides with the position of the pole if the zero appears below the threshold for decay into quark pairs. Another prescription for the mass would be to take the real part of the complex pole of the meson propagator, yielding a somewhat different result, or to compute the spectral function whose peak position and broadness indicate the physical mass and

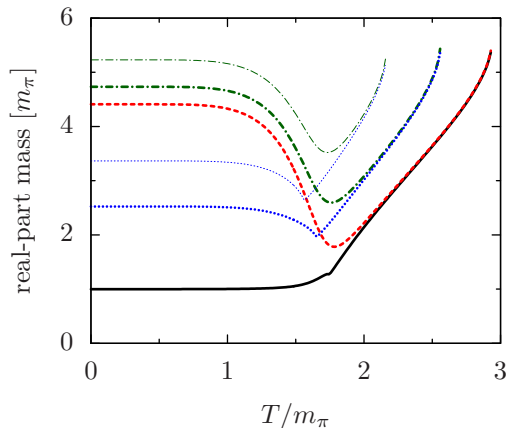


FIG. 6: Meson real-part masses at $\mu_B = 0$ as a function of T/m_π . The notation for the lines is the same as in Fig. 5: The black solid is m_π , the red dashed m_σ , the blue dotted m_η , and the green dash-dotted m_a . The thick lines correspond to m_η and m_a at $\alpha = 0.05$, while the thin lines to $\alpha = 0.1$.

decay width.

In the $U(1)_A$ -symmetric limit ($\alpha = 0$), in our calculations, the masses of η_0 and a_0 are equal to those of π and σ , respectively. The degeneracy of η_0 and π is generally exact only when the quark mass is strictly zero, so that they are both massless NG bosons. In the (P)NJL model in the mean-field approximation, this exact degeneracy holds regardless of finite quark masses, which is an artifact of the approximation. In fact, η_0 and π belong to different irreducible representations of the unbroken $SO(5)$; η_0 is a singlet and π (with Δ) form a quintet. The degeneracy is only approximate for small quark mass once higher-order meson loops are taken into account.

Off the limit of $\alpha = 0$, both m_η and m_a increase steeply. The typical value of α in the three-color NJL model with two light quark flavors, that one can obtain either by fitting the physical η' mass or by a reduction of the three-flavor model, is in the range 0.1 – 0.2 [74]. In order to be able to investigate the convergence to the $U(1)_A$ -symmetric limit, we consider in the following two particular values, $\alpha = 0.05$ and $\alpha = 0.1$. That is, if we assume that the vacuum value is $\alpha \simeq 0.1$, we consider two examples of no reduction at all and 50% reduction of $U(1)_A$ effects. It is quite unlikely that α goes to zero in the T and μ_B range of our interest.

In Fig. 6 the meson real-part masses are plotted as a function of T/m_π while keeping $\mu_B = 0$. The reason why some curves exhibit a cusp structure is that the corresponding modes cross the quark–antiquark (or quark–quark in the case of diquarks) threshold as T increases (and M decreases accordingly). Of course, such a decay into quarks is unphysical and is just an artifact, following from the lack of confinement in the NJL model. Even in the PNJL model these decay processes are not sufficiently suppressed [69], since the coupling to the Polyakov loop only imitates confinement in a statistical sense.

The real-part masses are difficult to measure on the lat-

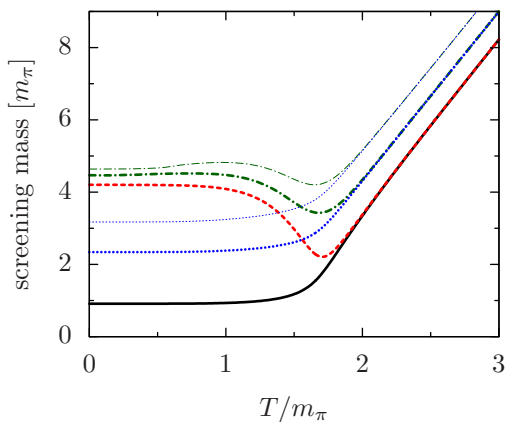


FIG. 7: Meson screening masses at $\mu_B = 0$ as a function of T/m_π . The notation for the lines is the same as in Fig. 5. The black solid is m_π , the red dashed m_σ , the blue dotted m_η , and the green dash-dotted m_a . The thick lines correspond to m_η and m_a at $\alpha = 0.05$, while the thin lines to $\alpha = 0.1$.

tice because the number of lattice sites in the temporal direction is severely limited. Instead, one can straightforwardly determine the damping of correlators of the fermion-bilinear interpolating fields for the mesons at large *spatial* separations. The exponential decay of the correlations is related to the screening mass of the lightest mode in the selected channel. In the (P)NJL model, this can be found as the pole of the static propagator, $D(\omega = 0, \mathbf{p})$, in the complex-momentum plane. The results are shown in Fig. 7. At $T = 0$ the real-part and screening masses should coincide thanks to the Lorentz invariance. In the model calculation, however, this nice feature is slightly breached by the three-momentum cut-off, but the difference of the two masses in the vacuum turns out to be about a few percent at most. Hence the apparent cutoff artifacts are reasonably small.

The masses of the chiral partners become degenerate at high temperature, signaling the restoration of chiral symmetry. On the other hand, at any (fixed) $\alpha \neq 0$ the masses of the parity partners, connected by a $U(1)_A$ rotation, do not converge even at the highest temperatures considered. From the technical point of view, this is a consequence of the simple structure of the inverse propagators (16): when chiral symmetry is restored, the self-energies of the parity partners become equal up to a simple rescaling by $\zeta^2 = (1 - 2\alpha)^2$. Physically, in reality, one should expect the coupling α to vary with T since it is induced by instantons whose density is exponentially suppressed at high T [50]. If we consider that the $U(1)_A$ -breaking interaction strength is proportional to the (pure) topological susceptibility, we can infer the T -dependence from the lattice data in the pure gauge simulation. Instead of doing so, in this work, we pick up several values of α .

A proper way to understand Fig. 7 is thus as follows. At $T = 0$ naturally α is nonzero, and if precise two-color simulation data is available for m_η and m_a , in princi-

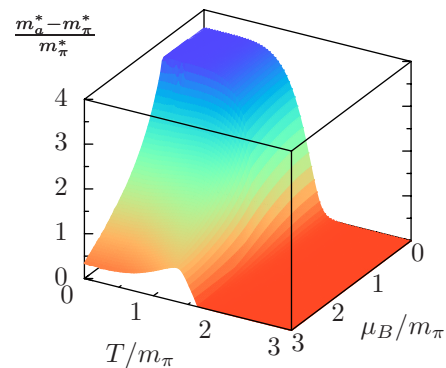


FIG. 8: Difference of the screening masses of a_0 and π as a function of μ_B/m_π and T/m_π in the extreme case of $\alpha = 0$. This quantity indicates the progressive $U(1)_A$ restoration in the hot and/or dense medium. The masses are denoted by m^* with asterisk to make clear that these are in-medium quantities and different from the vacuum m_π which is a fixed parameter of the model; see Table I.

ple, α can be fixed by the data. We can perform the PNJL model calculations using the determined α to go to the higher temperature. If we see a reduction of m_η and m_a toward degenerated m_π and m_σ , it is a signal for the effective $U(1)_A$ restoration. We can deduce how far α decreases by adjusting α to fit m_η and m_a at each temperature. Hence, Fig. 7 is a demonstration for all these possible investigations once the two-color simulation successfully measures the screening masses in good precision.

Finally, in Fig. 8, we plot the difference of screening masses of a_0 and π as a function of μ_B/m_π and T/m_π . Since these two modes do not mix even in presence of the diquark condensate, the masses can be calculated straightforwardly also in the BEC phase using the in-medium propagators (15). The choice of the screening masses instead of the real-part ones here is motivated by the lattice measurement, and also technically favored: while the real-part masses are obscured by Landau damping in the diquark condensation phase at $T \neq 0$, the screening masses remain well defined. The results indicate effective restoration of $U(1)_A$ symmetry at high temperature and/or chemical potential. While in the T -direction the degeneracy more-or-less copies the restoration of chiral symmetry which is another source of $U(1)_A$ breaking, in the μ_B -direction the convergence of m_a^* and m_π^* is slower as a result of additional $U(1)_A$ breaking by the diquark condensate. We note that Fig. 8 is the extreme example of $\alpha = 0$, which is not likely near the phase boundaries, but could be the case in the quark-gluon plasma region in view of the lattice data of the topological susceptibility [83]. In the future, by combining the two-color lattice outputs and the PNJL model analysis, it would be possible to make a 3D plot of α which should approach zero at high T and/or high μ_B .

IV. CONCLUSIONS

We have adopted the PNJL model as an effective approach to two-color QCD and applied it to the case of two light quark flavors. This is the simplest case which exhibits nontrivial low-energy spectrum due to spontaneous chiral symmetry breaking, and at the same time can be simulated by lattice Monte-Carlo techniques. We argued that one can fit the parameters of the NJL part of the model using physical (three-color) observables, but their values have to be rescaled appropriately. Once this is done and the quark sector is coupled to the Polyakov loop, the model yields locking behavior of chiral and deconfinement crossovers as long as μ_B is zero.

We checked older results on the phase structure of the two-color NJL model in the plane of T/m_π and μ_B/m_π , and analyzed its modification induced by the coupling to the Polyakov loop. The phase transition between the normal and superfluid phases is second order for all values of the chemical potential considered. In a large part of the diquark condensation phase the expectation value of the Polyakov loop is small, which resembles quarkyonic matter predicted using large- N_c arguments. We carefully clarified the realization of quarkyonic matter in the two-color system. The baryon number density n_B appears finite as soon as μ_B exceeds the mass of the baryonic pion, but still the quark contribution to n_B is not substantial until μ_B surpasses the twice of the dynamical quark mass. After then quark degrees of freedom supersede baryons, meaning a transition from “superfluid nuclear matter” into “quarkyonic superfluid.”

Our model analysis of the phase diagram is based on two simplifying assumptions. The first one is the mean-field approximation which treats the system as a gas of noninteracting fermionic quasiparticles. This may not be quantitatively accurate in some regions of the phase diagram such as for $\mu_B \simeq m_\pi$ at nonzero temperature where the system behaves rather as a dilute Bose gas. On the other hand, in the theory of strongly-interacting Fermi gases the mean-field approximation is known to be reliable at zero temperature. Moreover, the structure of the phase diagram concerning diquark condensation and chiral symmetry restoration is robust, being a direct consequence of the symmetry of two-color QCD. The second assumption is the extrapolation of the gauge part of the thermodynamic potential to nonzero baryon chemical potential. This has been justified for three-color QCD and low baryon chemical potential by a comparison with available lattice data and, in fact, is the source of the predictive power of the PNJL model. Therefore, we are confident about the existence of the quarkyonic superfluid phase as depicted in Fig. 1. On the other hand, the most recent lattice data [32] suggest that the Polyakov loop at a fixed low value of temperature starts to rise at $\mu_B \gtrsim 3m_\pi$, signalling possible deconfinement. This certainly presents a challenge to the PNJL model and determines the direction of our future research efforts.

Finally, we studied the dependence of the spectrum

of collective excitations (scalar and pseudoscalar mesons and diquarks) on the strength of the axial anomaly. For that sake we introduced a NJL-type interaction with a tunable $U(1)_A$ -breaking parameter. For all modes we calculated both the real-part mass and the screening mass, which governs the decay of spatial correlators, in order to facilitate a direct comparison with lattice simulations. Above the chiral restoration/deconfinement temperature the masses of the chiral partners become degenerate, as expected. At the same time, our results indicate that the restoration of $U(1)_A$ symmetry in terms of the masses of parity partners cannot be hidden by chiral restoration unlike the full topological susceptibility, which is good. This would naturally incorporate in the model study the suppression of instanton effects in a hot and/or dense matter. To make this whole argument into a quantitative predictive framework, further physical input from the lattice simulation would be indispensable, e.g. precise measurement of m_a as a function of T and μ_B . It would be also interesting that, since the topological susceptibility in the two-color pure gauge theory does not cost much, we can compare the inferred α behavior and the suppression of the pure topological susceptibility.

Acknowledgments

The authors are grateful to H. Abuki, J. O. Andersen, X. Huang, L. Kyllingstad, and W. Weise for useful discussions, and to L. He for pointing out an error in an earlier version of the manuscript. The work of T. B. was supported in part by the Alexander von Humboldt Foundation, and by the ExtreMe Matter Institute EMMI in the framework of the Helmholtz Alliance Program of the Helmholtz Association (HA216/EMMI). K. F. is supported by Japanese MEXT grant No. 20740134 and also supported in part by Yukawa International Program for Quark Hadron Sciences. Y. H. was supported by the Grant-in-Aid for the Global COE Program “The Next Generation of Physics, Spun from Universality and Emergence” from the MEXT of Japan.

Appendix: Ginzburg–Landau expansion of the thermodynamic potential

In order to make clear whether the phase transition of diquark superfluidity becomes (weakly) first order at high μ_B , we performed the Ginzburg–Landau expansion of the thermodynamic potential near the second-order transition line and calculated the coefficient of the quartic term with respect to Δ . In the presence of a tricritical point and the onset of a first-order phase transition, this coefficient would go to zero and then change its sign to negative.

The thermodynamic potential Ω depends only on the square of the diquark condensate. In general, Ω depends on other condensates, symbolically denoted by χ_a , as

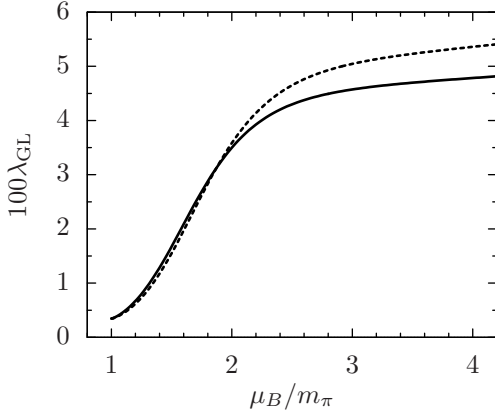


FIG. 9: Ginzburg–Landau quartic coupling along the second-order transition line as a function of μ_B/m_π . The solid and dashed lines are the PNJL and NJL model results, respectively, with the same input parameters.

well. In the PNJL model, we have $\chi = \{\sigma, \Phi\}$, while in the standard NJL model the only other condensate would be σ . To study the behavior of the diquark condensate near the critical temperature, it is most convenient to solve the gap equations for the other condensates, i.e., $\partial\Omega/\partial\chi_a = 0$. These define χ_a implicitly as a function of Δ^2 , and the thermodynamic potential is then a function of Δ^2 solely, that is, $\Omega = \Omega(\Delta^2, \chi_a(\Delta^2))$.

The coefficients of the quadratic and quartic terms in the Ginzburg–Landau functional are now determined by the first and second *total* derivatives with respect to Δ^2 , evaluated at $\Delta = 0$. The first derivative vanishes at the transition point by means of the gap equation. The second derivative defines the effective Ginzburg–Landau quartic coupling and is in general expressed as

$$\begin{aligned} \lambda_{\text{GL}} &= \frac{d^2\Omega}{d(\Delta^2)^2} \\ &= \frac{\partial^2\Omega}{\partial(\Delta^2)^2} - \frac{\partial^2\Omega}{\partial\Delta^2\partial\chi_a} \left(\frac{\partial^2\Omega}{\partial\chi_a\partial\chi_b} \right)^{-1} \frac{\partial^2\Omega}{\partial\chi_b\partial\Delta^2}. \end{aligned} \quad (17)$$

The inverse in the second term is assumed in the matrix

sense. The sign of λ_{GL} decides whether the transition is of first or second order. In particular in the NJL model, this expression acquires a simple form (with an obvious notation for the partial derivatives)

$$\lambda_{\text{GL}}^{\text{NJL}} = \partial_{\Delta^2\Delta^2}\Omega - \frac{(\partial_{\Delta^2\sigma}\Omega)^2}{\partial_{\sigma\sigma}\Omega}. \quad (18)$$

In the PNJL model, one has to calculate the 3×3 matrix of second partial derivatives. Given the formula for the thermodynamic potential (9), these are easily evaluated explicitly at $\Delta = 0$ as,

$$\begin{aligned} \partial_{\Delta^2\Delta^2}\Omega &= \sum_{i=\pm} \int \frac{d^3\mathbf{k}}{(2\pi)^3} \frac{\varphi(\xi_{\mathbf{k}}^i) - \xi_{\mathbf{k}}^i \varphi'(\xi_{\mathbf{k}}^i)}{(\xi_{\mathbf{k}}^i)^3}, \\ \partial_{\Delta^2\sigma}\Omega &= 2M \sum_{i=\pm} \int \frac{d^3\mathbf{k}}{(2\pi)^3} \frac{\varphi(\xi_{\mathbf{k}}^i) - \xi_{\mathbf{k}}^i \varphi'(\xi_{\mathbf{k}}^i)}{\epsilon_{\mathbf{k}}(\xi_{\mathbf{k}}^i)^2}, \\ \partial_{\Delta^2\Phi}\Omega &= 2 \sum_{i=\pm} \int \frac{d^3\mathbf{k}}{(2\pi)^3} \frac{\sinh \beta \xi_{\mathbf{k}}^i}{\xi_{\mathbf{k}}^i (\cosh \beta \xi_{\mathbf{k}}^i + \Phi)^2}, \\ \partial_{\sigma\sigma}\Omega &= \frac{1}{2G} \frac{m_0}{M} + 4M^2 \sum_{i=\pm} \int \frac{d^3\mathbf{k}}{(2\pi)^3} \frac{\varphi(\xi_{\mathbf{k}}^i) - \epsilon_{\mathbf{k}} \varphi'(\xi_{\mathbf{k}}^i)}{\epsilon_{\mathbf{k}}^3}, \\ \partial_{\sigma\Phi}\Omega &= 4M \sum_{i=\pm} \int \frac{d^3\mathbf{k}}{(2\pi)^3} \frac{\sinh \beta \xi_{\mathbf{k}}^i}{\epsilon_{\mathbf{k}} (\cosh \beta \xi_{\mathbf{k}}^i + \Phi)^2}, \\ \partial_{\Phi\Phi}\Omega &= 2bT \left[\frac{1 + \Phi^2}{(1 - \Phi^2)^2} - 24e^{-\beta a} \right] \\ &\quad + 4T \sum_{i=\pm} \int \frac{d^3\mathbf{k}}{(2\pi)^3} \frac{1}{(\cosh \beta \xi_{\mathbf{k}}^i + \Phi)^2}. \end{aligned} \quad (19)$$

The NJL limit is recovered by setting $\Phi \rightarrow 1-$.

We plot the numerical results in Fig. 9, from which we conclude that the Ginzburg–Landau coupling is always positive, and that the phase transition hence is always second order, within a reasonable chemical potential range (below the cutoff Λ), and in both NJL and PNJL models.

-
- [1] S. Muroya, A. Nakamura, C. Nonaka, and T. Takaishi, Prog. Theor. Phys. **110**, 615 (2003), hep-lat/0306031.
 - [2] M. G. Alford, A. Kapustin, and F. Wilczek, Phys. Rev. **D59**, 054502 (1999), hep-lat/9807039.
 - [3] P. de Forcrand and O. Philipsen, Nucl. Phys. **B642**, 290 (2002), hep-lat/0205016.
 - [4] M. D’Elia and M.-P. Lombardo, Phys. Rev. **D67**, 014505 (2003), hep-lat/0209146.
 - [5] P. de Forcrand and O. Philipsen, Nucl. Phys. **B673**, 170 (2003), hep-lat/0307020.
 - [6] M. D’Elia and M. P. Lombardo, Phys. Rev. **D70**, 074509 (2004), hep-lat/0406012.
 - [7] H.-S. Chen and X.-Q. Luo, Phys. Rev. **D72**, 034504 (2005), hep-lat/0411023.
 - [8] V. Azcoiti, G. Di Carlo, A. Galante, and V. Laliena, Nucl. Phys. **B723**, 77 (2005), hep-lat/0503010.
 - [9] P. de Forcrand and O. Philipsen, JHEP **01**, 077 (2007), hep-lat/0607017.
 - [10] L.-K. Wu, X.-Q. Luo, and H.-S. Chen, Phys. Rev. **D76**, 034505 (2007), hep-lat/0611035.
 - [11] M. D’Elia, F. Di Renzo, and M. P. Lombardo, Phys. Rev. **D76**, 114509 (2007), arXiv:0705.3814 [hep-lat].
 - [12] P. de Forcrand and O. Philipsen, JHEP **11**, 012 (2008), arXiv:0808.1096 [hep-lat].
 - [13] M. D’Elia and F. Sanfilippo (2009), arXiv:0904.1400 [hep-lat].

- [14] D. T. Son and M. A. Stephanov, Phys. Rev. Lett. **86**, 592 (2001), hep-ph/0005225.
- [15] J. B. Kogut and D. K. Sinclair, Phys. Rev. **D66**, 034505 (2002), hep-lat/0202028.
- [16] J. B. Kogut and D. K. Sinclair, Phys. Rev. **D70**, 094501 (2004), hep-lat/0407027.
- [17] J. B. Kogut, M. A. Stephanov, D. Toublan, J. J. M. Verbaarschot, and A. Zhitnitsky, Nucl. Phys. **B582**, 477 (2000), hep-ph/0001171.
- [18] K. Splittorff, D. T. Son, and M. A. Stephanov, Phys. Rev. **D64**, 016003 (2001), hep-ph/0012274.
- [19] S. Hands et al., Eur. Phys. J. **C17**, 285 (2000), hep-lat/0006018.
- [20] S. Hands, I. Montvay, L. Scorzato, and J. Skullerud, Eur. Phys. J. **C22**, 451 (2001), hep-lat/0109029.
- [21] A. Nakamura, Phys. Lett. **B149**, 391 (1984).
- [22] J. B. Kogut, M. A. Stephanov, and D. Toublan, Phys. Lett. **B464**, 183 (1999), hep-ph/9906346.
- [23] J. B. Kogut, D. K. Sinclair, S. J. Hands, and S. E. Morrison, Phys. Rev. **D64**, 094505 (2001), hep-lat/0105026.
- [24] S. Muroya, A. Nakamura, and C. Nonaka, Phys. Lett. **B551**, 305 (2003), hep-lat/0211010.
- [25] J. B. Kogut, D. Toublan, and D. K. Sinclair, Phys. Rev. **D68**, 054507 (2003), hep-lat/0305003.
- [26] J.-I. Skullerud, S. Ejiri, S. Hands, and L. Scorzato, Prog. Theor. Phys. Suppl. **153**, 60 (2004), hep-lat/0312002.
- [27] P. Giudice and A. Papa, Phys. Rev. **D69**, 094509 (2004), hep-lat/0401024.
- [28] S. Chandrasekharan and F.-J. Jiang, Phys. Rev. **D74**, 014506 (2006), hep-lat/0602031.
- [29] S. Hands, S. Kim, and J.-I. Skullerud, Eur. Phys. J. **C48**, 193 (2006), hep-lat/0604004.
- [30] P. Cea, L. Cosmai, M. D'Elia, and A. Papa, Phys. Rev. **D77**, 051501 (2008), arXiv:0712.3755 [hep-lat].
- [31] S. Hands, P. Sitch, and J.-I. Skullerud, Phys. Lett. **B662**, 405 (2008), arXiv:0710.1966 [hep-lat].
- [32] S. Hands (2008), talk at "Tools for Finite Density QCD", November 19-21, 2008, Bielefeld.
- [33] M.-P. Lombardo, M. L. Paciello, S. Petrarca, and B. Taglienti, Eur. Phys. J. **C58**, 69 (2008), arXiv:0804.4863 [hep-lat].
- [34] R. Rapp, T. Schaefer, E. V. Shuryak, and M. Velkovsky, Phys. Rev. Lett. **81**, 53 (1998), hep-ph/9711396.
- [35] A. Smilga and J. J. M. Verbaarschot, Phys. Rev. **D51**, 829 (1995), hep-th/9404031.
- [36] K. Splittorff, D. Toublan, and J. J. M. Verbaarschot, Nucl. Phys. **B620**, 290 (2002), hep-ph/0108040.
- [37] K. Splittorff, D. Toublan, and J. J. M. Verbaarschot, Nucl. Phys. **B639**, 524 (2002), hep-ph/0204076.
- [38] T. Kanazawa, T. Wettig, and N. Yamamoto (2009), arXiv:0906.3579 [hep-ph].
- [39] J. T. Lenaghan, F. Sannino, and K. Splittorff, Phys. Rev. **D65**, 054002 (2002), hep-ph/0107099.
- [40] J. Wirstam, J. T. Lenaghan, and K. Splittorff, Phys. Rev. **D67**, 034021 (2003), hep-ph/0210447.
- [41] B. Vanderheyden and A. D. Jackson, Phys. Rev. **D64**, 074016 (2001), hep-ph/0102064.
- [42] B. Klein, D. Toublan, and J. J. M. Verbaarschot, Phys. Rev. **D72**, 015007 (2005), hep-ph/0405180.
- [43] Y. Shinno and H. Yoneyama (2009), arXiv:0903.0922 [hep-lat].
- [44] E. Dagotto, F. Karsch, and A. Moreo, Phys. Lett. **B169**, 421 (1986).
- [45] S. Chandrasekharan, Phys. Rev. Lett. **97**, 182001 (2006), hep-lat/0608007.
- [46] Y. Nishida, K. Fukushima, and T. Hatsuda, Phys. Rept. **398**, 281 (2004), hep-ph/0306066.
- [47] K. Fukushima, JHEP **07**, 083 (2008), arXiv:0806.1104 [hep-ph].
- [48] C. Ratti and W. Weise, Phys. Rev. **D70**, 054013 (2004), hep-ph/0406159.
- [49] G. 't Hooft, Phys. Rev. Lett. **37**, 8 (1976).
- [50] D. J. Gross, R. D. Pisarski, and L. G. Yaffe, Rev. Mod. Phys. **53**, 43 (1981).
- [51] T. Schafer, Phys. Rev. **D65**, 094033 (2002), hep-ph/0201189.
- [52] R. D. Pisarski and F. Wilczek, Phys. Rev. **D29**, 338 (1984).
- [53] E. V. Shuryak, Comments Nucl. Part. Phys. **21**, 235 (1994), hep-ph/9310253.
- [54] K. Fukushima, K. Ohnishi, and K. Ohta, Phys. Rev. **C63**, 045203 (2001), nucl-th/0101062.
- [55] P. Costa, M. C. Ruivo, C. A. de Sousa, and Y. L. Kalinovsky, Phys. Rev. **D70**, 116013 (2004), hep-ph/0408177.
- [56] P. Costa, M. C. Ruivo, C. A. de Sousa, H. Hansen, and W. M. Alberico, Phys. Rev. **D79**, 116003 (2009), arXiv:0807.2134 [hep-ph].
- [57] S. Chandrasekharan and A. C. Mehta, Phys. Rev. Lett. **99**, 142004 (2007), arXiv:0705.0617 [hep-lat].
- [58] K. Fukushima, Phys. Rev. **D77**, 114028 (2008), arXiv:0803.3318 [hep-ph].
- [59] J.-W. Chen, K. Fukushima, H. Kohyama, K. Ohnishi, and U. Raha (2009), arXiv:0901.2407 [hep-ph].
- [60] L. McLerran and R. D. Pisarski, Nucl. Phys. **A796**, 83 (2007), arXiv:0706.2191 [hep-ph].
- [61] Y. Hidaka, L. D. McLerran, and R. D. Pisarski, Nucl. Phys. **A808**, 117 (2008), arXiv:0803.0279 [hep-ph].
- [62] T. Schafer and F. Wilczek, Phys. Rev. Lett. **82**, 3956 (1999), hep-ph/9811473.
- [63] M. G. Alford, J. Berges, and K. Rajagopal, Nucl. Phys. **B558**, 219 (1999), hep-ph/9903502.
- [64] K. Fukushima, Phys. Rev. **D70**, 094014 (2004), hep-ph/0403091.
- [65] T. Hatsuda, M. Tachibana, N. Yamamoto, and G. Baym, Phys. Rev. Lett. **97**, 122001 (2006), hep-ph/0605018.
- [66] K. Fukushima, Phys. Lett. **B591**, 277 (2004), hep-ph/0310121.
- [67] C. Ratti, M. A. Thaler, and W. Weise, Phys. Rev. **D73**, 014019 (2006), hep-ph/0506234.
- [68] S. Roessner, C. Ratti, and W. Weise, Phys. Rev. **D75**, 034007 (2007), hep-ph/0609281.
- [69] H. Hansen, W. M. Alberico, A. Beraudo, A. Molinari, M. Nardi, and C. Ratti, Phys. Rev. **D75**, 065004 (2007), hep-ph/0609116.
- [70] C. Sasaki, B. Friman, and K. Redlich, Phys. Rev. **D75**, 074013 (2007), hep-ph/0611147.
- [71] S. Roessner, T. Hell, C. Ratti, and W. Weise, Nucl. Phys. **A814**, 118 (2008), arXiv:0712.3152 [hep-ph].
- [72] H. Abuki, M. Ciminale, R. Gatto, G. Nardulli, and M. Ruggieri, Phys. Rev. **D77**, 074018 (2008), arXiv:0802.2396 [hep-ph].
- [73] B.-J. Schaefer, J. M. Pawłowski, and J. Wambach, Phys. Rev. **D76**, 074023 (2007), arXiv:0704.3234 [hep-ph].
- [74] M. Buballa, Phys. Rept. **407**, 205 (2005), hep-ph/0402234.
- [75] G.-F. Sun, L. He, and P. Zhuang, Phys. Rev. **D75**, 096004 (2007), hep-ph/0703159.

- [76] C. Vafa and E. Witten, Phys. Rev. Lett. **53**, 535 (1984).
- [77] D. Boer and J. K. Boomsma, Phys. Rev. **D78**, 054027 (2008), arXiv:0806.1669 [hep-ph].
- [78] H. Abuki and K. Fukushima, Phys. Lett. **B676**, 57 (2009), arXiv:0901.4821 [hep-ph].
- [79] H. Abuki, R. Anglani, R. Gatto, G. Nardulli, and M. Ruggieri, Phys. Rev. **D78**, 034034 (2008), arXiv:0805.1509 [hep-ph].
- [80] P. Hegde, F. Karsch, E. Laermann, and S. Shcheredin, Eur. Phys. J. **C55**, 423 (2008), arXiv:0801.4883 [hep-lat].
- [81] L. McLerran, K. Redlich, and C. Sasaki, Nucl. Phys. **A824**, 86 (2009), arXiv:0812.3585 [hep-ph].
- [82] T. Hatsuda and T. Kunihiro, Phys. Rept. **247**, 221 (1994), hep-ph/9401310.
- [83] B. Alles, M. D'Elia, and M. P. Lombardo, Nucl. Phys. **B752**, 124 (2006), hep-lat/0602022.